Comparison of post-process X-ray computed tomography and in-process optical measurements for defects evaluation in additively manufactured parts

Nicolò Bonato[1], Filippo Zanini[1], Simone Carmignato[1]

[1]University of Padova, Stradella San Nicola 3, Vicenza, Italy, e-mail: nicolo.bonato@phd.unipd.it | filippo.zanini@unipd.it | simone.carmignato@unipd.it

Abstract

Despite the capability of fabricating complex and customized components, metal laser powder bed fusion (LPBF) is still affected by manufacturing issues, which can lead to significant geometrical and dimensional errors and internal defects. These aspects can represent a major barrier to a wider industrial application of LPBF, particularly if considering that relevant applications of additive manufacturing are in sectors such as biomedical and aerospace, which have stringent requirements in terms of defects and product quality. The requests for precision improvement are orienting research activities towards the development of in-process monitoring systems able to perform accurate analyses during the fabrication itself, hence providing useful information for improving the quality of produced parts. To this aim, several in-process monitoring methods have been proposed in the literature to identify and correct out-of-control process conditions. In spite of the aforementioned research efforts, work is still needed to reliably correlate in-process measurements to actual defects. The focus of this experimental study is the definition of a robust methodology to compare in-process optical acquisitions to post-process X-ray computed tomography (XCT) measurements of actual defects. XCT unique capabilities are therefore exploited to support and improve the LPBF process through the implementation of an accurate comparison methodology.

Keywords: X-ray computed tomography, additive manufacturing, dimensional metrology, defect analysis, in-process optical measurements

1 Introduction

Metal additive manufacturing (AM) is gaining increasing academic and industrial interest due to several advantages, such as efficient material use, manufacturability of complex and customized geometries, and enhanced performance-driven engineering design [1]. Moreover, the inherent flexibility of this production technology allows a faster industrial reconversion, increasing companies' resilience against market changes or other unpredictable events [2].

In particular, this experimental work is focused on laser powder bed fusion (LPBF) of metals, an additive manufacturing technology where the feedstock material is in form of a metal powder that is spread on a building platform to generate the so-called powder bed, which is then processed under the action of a laser. The laser selectively melts the powder at specified locations, generating a material consolidated layer as soon as metal solidification is completed. The process is then repeated iteratively by adding one layer at a time until the entire geometry is completed.

Despite the aforementioned advantages, metal LPBF typically suffers from defects formation during the fabrication, including internal porosities. The most common internal flaws are known as lack-of-fusion defects, which are a consequence of the insufficient melting of powders. Those defects can be clearly identified due to the considerable size and their characteristic irregular form, therefore resulting particularly critical, for example for fatigue resistance [3]. The discussed issues constitute a major barrier for a wider adoption of the LPBF technology, especially in industrial sectors with demanding standard requirements such as aerospace and biomedical [4]. For this reason, reliable metrology solutions are currently needed to improve the understanding of LPBF process dynamics and to gain control over the process stability [5]. In this context, X-ray computed tomography (XCT) is an attractive solution for non-destructive and holistic post-process evaluations of AM specimens, including dimensional and geometrical measurements as well as internal porosity analysis [6]. In order to effectively exploit XCT evaluations for process development, the obtained results should be used to study their correlation with specific process dynamics and issues, with the aim to prevent future process anomalies and subsequent product failures or rejection caused by unacceptable defect rates or geometrical inaccuracies [6]. An interesting opportunity that is gaining increasing attention is the possibility of combining XCT post-process measurements with real-time monitoring data on phenomenon and anomalies occurring during the LPBF process [7]. This combination has two main objectives: improving the understanding of LPBF process, and validating the data acquired on a layer basis during the process, e.g. to take smart and corrected actions through a feedback control loop operating on the process itself, towards first-time-right manufacturing.

Several in-process monitoring systems have already been proposed in the literature, each of them gathering information linked to different process levels (e.g. powder bed, scan tracks, melt pool, under the layer) [8, 9, 10]. However, despite the efforts, research work is still needed to reliably correlate the acquired signals to the actual flaws [11]. On one side, anomalies detected during the process can be altered when generating the successive layers of material. On the other side, the accurate registration of in-process and post-process data – which is necessary for a reliable comparison – can be complicated for example by the occurrence of after-build shrinkage and/or deformations.

https://doi.org/10.58286/26623

The purpose of this study regards the development of an adequate and robust methodology to compare in-process signals gathered by optical image acquisition during the LPBF process with actual defects measured by XCT on the fabricated parts, as reported in Figure 1.

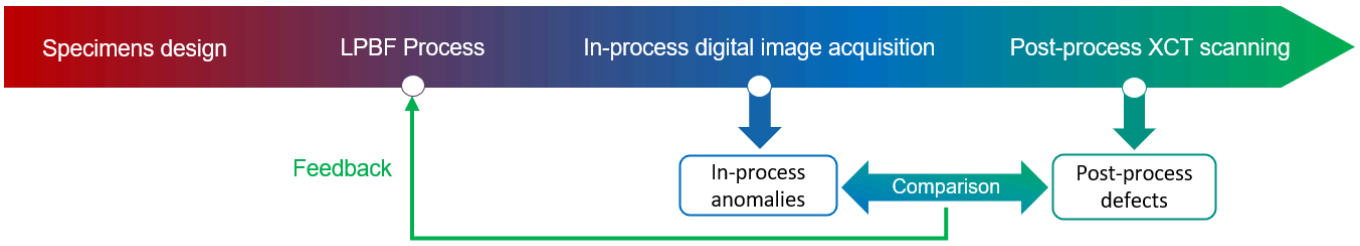

Figure 1: Schematic of the proposed methodology showing the comparison between in-process optically detected anomalies and post-process XCT measured defects. The comparison is needed to provide robust feedback to the LPBF process and considers both outer geometry and inner defects.

2 Material and methods

This section describes the materials and methods used for LPBF process monitoring and for the detection and comparison between in-process monitoring data and post-process measurement results.

2.1 Configuration of the in-process monitoring system

The in-process monitoring system developed in this work is part of the level 1 monitoring, which aims at analysing the quality of powder bed and fabricated layers [7]. For this reason, digital images of a field of view that includes the entire building platform were captured. More specifically, two images were collected for each layer, one after the recoating action, and the other one right after the laser scanning. This work specifically focuses on the latter analysis only.

The system architecture, outlined in Figure 2, includes a 18 megapixel digital single-lens reflex camera installed with a tilted optical axis with respect to the laser beam direction and a side raking light that highlights possible out-of-plane anomalies (e.g. lack-of-fusion defects or protruding features) as well as in-plane geometrical defects. This camera configuration is commonly known as *off-axis positioning* [12] and implies the need to correct perspective deformations in the images. In order to perform this operation, a calibrated hole plate was imaged onto the build platform using the same optical setup before starting the fabrication. The warped image of the hole plate was therefore corrected using a specific routine developed in MATLAB (Mathworks, USA) through the determination of the transformation matrix T given in Equation (2.1), as described in [13]:

$$\boldsymbol{T} = \begin{bmatrix} a_{11} & a_{12} & a_{13} \\ a_{21} & a_{22} & a_{23} \\ a_{31} & a_{32} & a_{33} \end{bmatrix}, \tag{2.1}$$

where a_{ij} is a generic element to be determined. Hence, the image correction takes place according to Equation (2.2):

$$[x' \quad y' \quad w'] = [u \quad v \quad 1] \cdot \boldsymbol{T}, \tag{2.2}$$

where $[u \quad v]$ and $\left[\frac{x'}{w'} \quad \frac{y'}{w'}\right]$ represent the coordinates in the original image space and the coordinate in the orthogonal object space, respectively [14]. The calibrated distances between the hole plate's holes were used to determine the transformation matrix T from equation (2.2). The derived transformation was then applied to correct the warping on the layer images acquired during manufacturing (see an example in Figures 3b and 3c). The pixel size of the corrected images was determined to be equal to 15 µm.

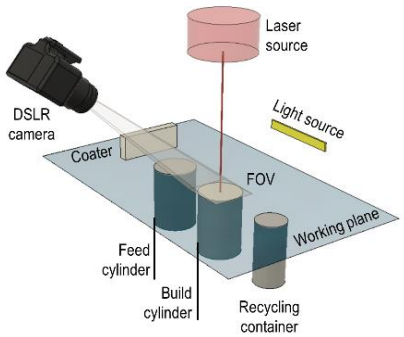

Figure 2: Schematic representation of the in-process monitoring setup.

2.2 Specimens design and fabrication

The specimens were designed as schematically represented in Figure 3a, to promote the accurate alignment between layers data acquired during the LPBF process and the corresponding cross-sections of the fabricated parts reconstructed by XCT. For this purpose, sections #1 and #2 (see Figure 3a) were conceived to avoid any symmetry. Cylindrical shapes (sections #3 and #4) were instead added on the top to better study the effect related to the light rays' direction with respect to the optical axis used for image acquisition. The specimens' outer envelope was chosen to be a 5 mm × 5 mm × 7 mm box, to enable XCT scanning at micrometric voxel size with the used XCT device (see Section 2.4). Furthermore, the unsupported region of transition between sections #1 and #2 was purposely included in the design for comparing in-process and post-process evaluations when complex process dynamics occur, such as in the case of unsupported overhangs.

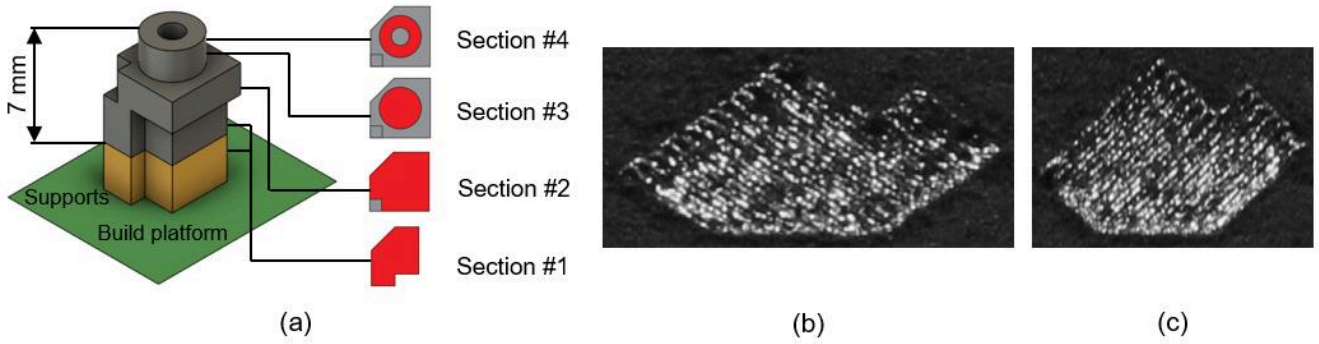

Figure 3: Geometry of the fabricated samples (a); optical image of a section 1 layer as acquired in-process by the camera (b); image of the same layer after the perspective correction operation (c).

Specimens were produced via LPBF of Ti6Al4V using a Sisma MYSINT100 system (Sisma SpA, Italy) by varying the process parameters through a progressive reduction of the input energy density in order to stimulate the formation of different types of defects. This paper especially focuses on lack-of-fusion defects, typically characterized by an irregular shape and by the presence of entrapped powder resulting from an inadequate melting of the powder bed. In such cases, because of the presence of powder, anomalies in the acquired optical images are expected to appear darker than molten regions due to their lower reflectivity; consequently they can be thresholded based on grey-level intensity as described in Section 2.3.

2.3 In-process optical measurements

The optical images acquired after the laser action were used to identify: (1) the actual contour of each layer and (2) the possible internal sites of porosity. In the first case, the image segmentation was carried out through a local-adaptive segmentation algorithm [15], which iteratively modifies the starting contour (obtained from the nominal geometry of each analysed layer) on the basis of the variations of grey levels detected along with a specified search distance. Prior to this procedure, a Gaussian filter was applied to all images to help the algorithm improve the estimation of local intensity value, as described in [16]. An example of contour determination of a layer is reported in Figure 4a,b. The segmentation routine was performed on all the layers of the sample and the obtained contours were vertically stacked with a spacing equal to the nominal layer thickness to obtain a 3D point cloud. The point clouds were then aligned to the nominal CAD model using a procedure implemented in the software GOM Inspect (GOM GmbH, Germany) by performing a best-fitting operation. An example of the resulting aligned point cloud is shown in Figure 4c.

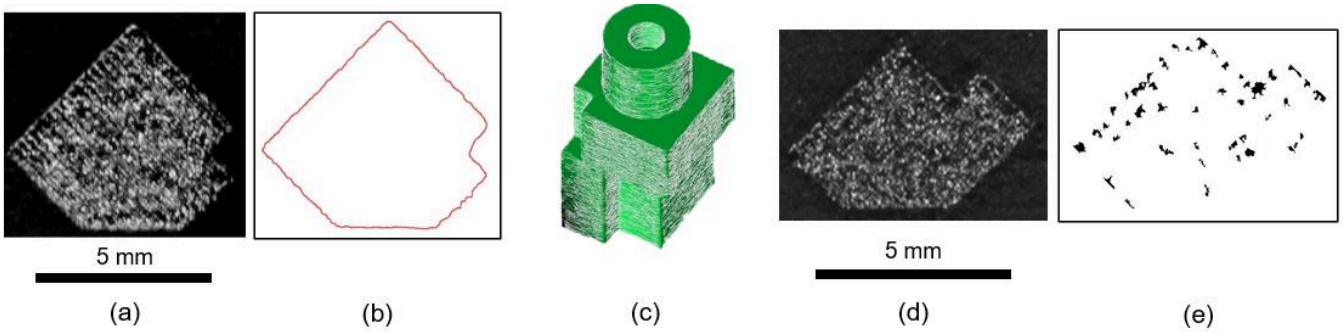

Figure 4: Layer image after perspective correction and pre-processing operations (a); contour segmentation of the same image (b); point cloud to CAD model alignment (c); image resulting from two layers as described by Equation 2.3 (d); outliers detected by thresholding the previous image (e).

Another thresholding operation was performed on the same images based on grey level intensity values, to detect possible internal anomalies. However, it is important to underline that the detected layer anomalies could sometimes lead to actual lack-of-fusion defects in the fabricated parts, but other times could be "cured" during the generation of successive layers as the laser typically has a penetration depth exceeding the nominal layer thickness. This aspect motivates the choice of considering couples of subsequent images to detect anomalies. In particular, the discrimination of an anomaly is performed by assuming that its extension spans at least across two layers, as reported in [17].
Each couple of images was elaborated to obtain a third image in which the brightness intensity *I(k)* for each pixel *k* is defined by the following equation:

$$I(k) = \max\big(I_n(k), I_{n+1}(k)\big), \tag{2.3}$$

where n and $n+1$ indicate the two images corresponding to the two consecutive layers. The resulting image was then thresholded based on the grey level intensity for the purpose of detecting low-brightness regions, which were therefore classified as anomalies as those shown in the example of Figure 4e.

2.4 Post-process XCT measurements

The fabricated specimens were scanned with a metrological XCT system (Nikon Metrology MCT225), equipped with a micro-focus X-ray source, a 16-bit X-ray detector with a 2000×2000 pixel grid, high-precision guideways and controlled cabinet temperature ($20 \pm 0.5\ °C$). The analysed samples were scanned using the parameters listed in Table 1, with a voxel size equal to 4.5 μm. A 0.1 mm copper physical filter was interposed between the X-ray source and the object in order to reduce beam hardening. Once the 1800 projections were acquired, they were exploited for reconstructing three-dimensional models of the scanned specimens.

Table 1 - XCT parameters

Parameter	Value
Voltage	180 kV
Current	38 µA
Power	6.8 W
Exposure time	2000 ms
Frames per projection	1
Nr. of projections	1800
Physical filter material	Cu
Physical filter thickness	0.1 mm
Voxel size	4.5 µm

Next to the reconstruction, the obtained volumes were analysed using the analysis and visualization software VGStudio MAX 3.2 (Volume Graphics GmbH), with the aim of identifying both the outer surface and the internal porosity. In particular, the surface was determined through the local-adaptive algorithm. XCT volumes were then aligned to the nominal CAD model to evaluate the actual to nominal deviations, as previously done with in-process gathered data (see Section 2.3).
Internal porosities were characterized in terms of dimension, shape and spatial positioning by means of the dedicated module of VGStudio MAX 3.2. Afterwards, the XCT cross-sections were extracted to be compared with the anomalies detected during the process in the corresponding layers.

3 Experimental results

In this section, the information gathered from in-process optical images is compared to the results obtained by post-process XCT measurements, with the purpose of evaluating potential correlations which are of great importance to reach a deeper understanding of LPBF defect formation mechanisms, thus improving the manufacturing process itself.
Figure 5a shows the deviation maps resulting from the CAD comparisons of 3D point clouds obtained from in-process data (top part of Figure 5a) and XCT reconstructions (bottom part of Figure 5a). Such comparisons show that major geometrical deviations can be successfully detected using in-process optical analyses, which means that they are generated during the LPBF process. Some regions show, instead, differences between deviations detected with in-process and post-process measurements. A part of such differences can be caused by the fact that some geometrical deformations only initiate from the cooling phase after the fabrication, and cannot be detected during the process. Other inconsistencies in the comparison can be due to the solid-sintering mechanism occurring after the layer completion, which can promote the attachment of powder to the outer surface and the part growth. In addition, the dross formation under overhang regions is a phenomenon occurring under the currently processed layer, so it cannot be anticipated by in-process sensing. The corner region above the overhang shows opposite colours obtained by in-process and post-process measurements. This is due to the fact that, when changing layer geometry from section #1 to section

#2, the surface folds up and the perspective correction does not consider possible out-of-plane deformations, hence resulting in an erroneous positive deviation.

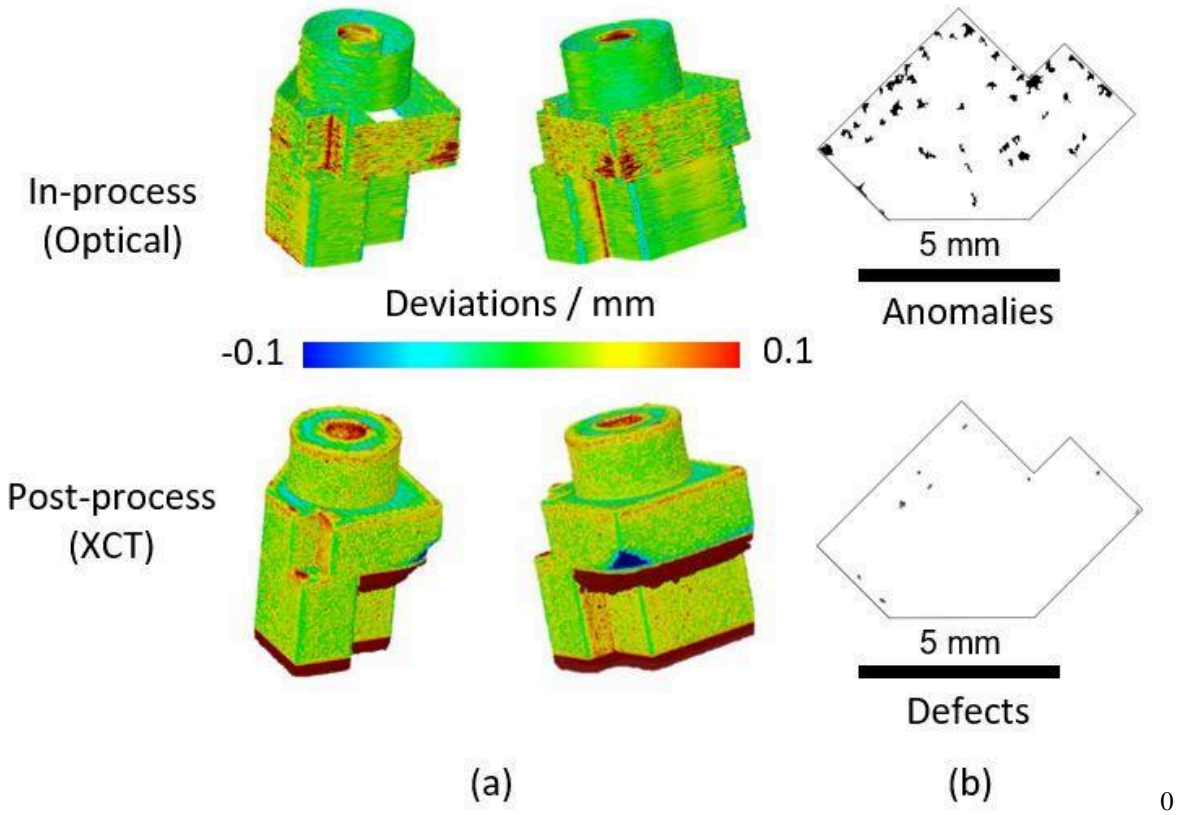

Figure 5: CAD comparison related to in-process optical monitoring and post-process XCT reconstruction (a); comparison of in-process detected anomalies and post-process defects in one layer (b).

Figure 5b shows the comparison between possible sites of internal defects revealed during the process and actual defects found by XCT during post-process inspection for a specimen manufactured with low energy density. A significant number of false positives was found, i.e. anomalies that are only detectable from optical images and that are not connected to any actual defects inside the part. With more specific regard to the specimen in Figure 5, almost 70 % of the lack-of-fusion pores detected by XCT was correctly revealed by analysing the in-process optical images, while the percentage of false positives was nearly 85 %, under the conditions of the preliminary experiments presented in this work. On one hand, as already explained above, the laser typically penetrates to a depth exceeding the nominal layer thickness, restoring some defects that were not completely molten at the time the optical image was acquired. On the other hand, the false positives may be related to the single lighting direction, which may result in the detection of dark areas which are shadows caused by the presence of super-elevated edges or by tilted surfaces preventing light reflectivity toward the optical sensor.

4 Conclusions and future work

This paper is focused on the development of a methodology to compare results from real-time LPBF process monitoring with results obtained by XCT post-process measurements. In this context, X-ray computed tomography acts not only as a flaw detection method, but also and more importantly as a fundamental tool for validating and further developing in-process monitoring solutions, hence effectively supporting metal additive manufacturing enhancement.

Thanks to the comparison with XCT data, the capability of the used monitoring system to successfully anticipate major geometrical defects was evaluated, as well as current limitations, which are visible for example in differences attributed to shrinkage and deformations occurring during the cool-down phase, due to residual stresses accumulated or due to artifacts caused by perspective correction. With regard to internal defects, under the conditions of the preliminary experiments presented in this work, 70 % of the actual porosities were properly revealed, while 85 % of false positives were also detected after image processing.

The combination of XCT post-process measurements with machine learning algorithms is expected to produce improvements of in-process monitoring and active process control, so this will be kept into consideration for future works. Regarding the improvement of defect detection rate with optical monitoring systems, multiple lights can be beneficial for false positives reduction and will be further investigated by comparing the obtained results with XCT post-process measurements.

References

[1] Dilberoglua U. M., Gharehpapagha B., Yaman U., Dolen M. (2017). The role of additive manufacturing in the era of industry 4.0, 27th International Conference on Flexible Automation and Intelligent Manufacturing, 27-30 June, Modena, Italy, https://doi.org/10.1016/j.promfg.2017.07.148.

[2] Naghshineh, B., Carvalho, H. (2022). The implications of additive manufacturing technology adoption for supply chain resilience: A systematic search and review, International Journal of Production Economics, https://doi.org/10.1016/j.ijpe.2021.1083.

[3] Benedetti M., Fontanari V., Bandini M., Zanini F., Carmignato S. (2018). Low- and high-cycle fatigue resistance of Ti-6Al-4V ELI additively manufactured via selective laser melting: Mean stress and defect sensitivity. International Journal of Fatigue 107:96-109, https://doi.org/10.1016/j.ijfatigue.2017.10.021.

[4] Gibson, I., Rosen, D., Stucker, B., Khorasani, M. (2021). Additive manufacturing technologies. New York: Springer.

[5] Leach R. K., Bourell D., Carmignato S., Donmez A., Senin N., Dewulf W. (2019). Geometrical metrology for metal additive manufacturing. CIRP Annals 68:677–700, https://doi.org/10.1016/j.cirp.2019.05.004.

[6] Leach R., Carmignato S., eds (2020), Precision Metal Additive Manufacturing. CRC Press, Boca Raton.

[7] Grasso M., Remani A., Dickins A., Colosimo B. M. (2021). In-situ measurement and monitoring methods for metal powder bed fusion – an updated review. Measurement Science and Technology 32, https://doi.org/10.1088/1361-6501/ac0b6b.

[8] Foster B. K., Reutzel E. W., Nassar A., Hall B. T., Brown S., Dickman C. (2015). Optical, layerwise monitoring of powder bed fusion. Solid Freedom Fabrication Symposium:295-307, 10-12 August, Austin (United States).

[9] Coeck S., Bisht M. (2019). Prediction of lack of fusion porosity in selective laser melting based on melt pool monitoring data. Additive Manufacturing 25:347-356, https://doi.org/10.1016/j.addma.2018.11.015.

[10] Kouprianoff, D., Yadroitsava, I., du Plessis, A., Luwes, N., & Yadroitsev, I. (2021). Monitoring of Laser Powder Bed Fusion by Acoustic Emission: Investigation of Single Tracks and Layers. Frontiers in Mechanical Engineering 7, https://doi.org/10.3389/fmech.2021.678076.

[11] Lu Q. Y., Nguyen N. V., Hum A. J. W., Tran T., Wong C. H. (2020). Identification and evaluation of defects in selective laser melted 316L stainless steel parts via in-situ monitoring and micro computed tomography. Additive Manufacturing 35, https://doi.org/10.1016/j.addma.2020.101287.

[12] Craeghs T., Bechman F., Berumen S., Kruth J. P. (2010). Feedback control of layerwise laser melting using optical sensors. Physics Procedia, 5:505–514, https://doi.org/10.1016/j.phpro.2010.08.078.

[13] Land W. S., Zhang B., Ziegert J., Davies A. (2015). In-Situ Metrology System for Laser Powder Bed Fusion. Procedia Manufacturing 1:393-403, https://doi.org/10.1016/j.promfg.2015.09.047.

[14] Wolberg G. (1990). Digital Image Warping. Los Alamitos (CA): IEEE Computer Society Press.

[15] Lankton S. (2008). Localizing Region-Based Active Contours. IEEE Trans Image Process 17:2029-2039, https://doi.org/10.1109/TIP.2008.2004611.

[16] Pagani L., Grasso M., Scott P. J., Colosimo B. M. (2020). Automated layerwise detection of geometrical distortions in laser powder. Additive Manufacturing 36, https://doi.org/10.1016/j.addma.2020.101435.

[17] Abdelrahman M., Reutzel E. W., Nassar A. R., Starr T. L. (2017). Flaw detection in powder bed fusion using optical imaging. Additive Manufacturing 15:1–11, https://doi.org/10.1016/j.addma.2017.02.001.